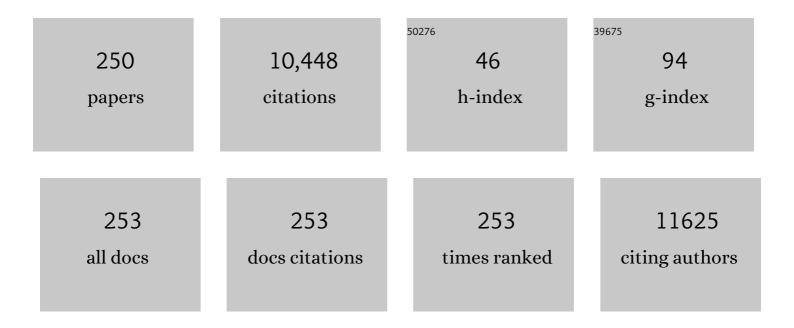
List of Publications by Year in descending order

Source: https://exaly.com/author-pdf/8130297/publications.pdf Version: 2024-02-01



IAN LIAVSKY

#	Article	IF	CITATIONS
1	<i>Irena</i> : tool suite for modeling and analysis of small-angle scattering. Journal of Applied Crystallography, 2009, 42, 347-353.	4.5	1,337
2	Anisotropic self-assembly of spherical polymer-grafted nanoparticles. Nature Materials, 2009, 8, 354-359.	27.5	925
3	<i>Nika</i> : software for two-dimensional data reduction. Journal of Applied Crystallography, 2012, 45, 324-328.	4.5	757
4	Glassy Carbon as an Absolute Intensity Calibration Standard for Small-Angle Scattering. Metallurgical and Materials Transactions A: Physical Metallurgy and Materials Science, 2010, 41, 1151-1158.	2.2	350
5	Ultra-small-angle X-ray scattering at the Advanced Photon Source. Journal of Applied Crystallography, 2009, 42, 469-479.	4.5	260
6	"Gel-like―Mechanical Reinforcement in Polymer Nanocomposite Melts. Macromolecules, 2010, 43, 1003-1010.	4.8	209
7	Comprehensive microstructural characterization and predictive property modeling of plasma-sprayed zirconia coatings. Acta Materialia, 2003, 51, 2457-2475.	7.9	207
8	Column Formation in Suspension Plasma-Sprayed Coatings and Resultant Thermal Properties. Journal of Thermal Spray Technology, 2011, 20, 817-828.	3.1	194
9	Protection of organic carbon in soil microaggregates via restructuring of aggregate porosity and filling of pores with accumulating organic matter. Geochimica Et Cosmochimica Acta, 2008, 72, 4725-4744.	3.9	157
10	Ultra-Small-Angle X-ray Scattering Instrument at the Advanced Photon Source: History, Recent Development, and Current Status. Metallurgical and Materials Transactions A: Physical Metallurgy and Materials Science, 2013, 44, 68-76.	2.2	139
11	A Phase Diagram for Polymer-Grafted Nanoparticles in Homopolymer Matrices. Macromolecules, 2012, 45, 4007-4011.	4.8	135
12	SAXS Study of the Nucleation of Glycine Crystals from a Supersaturated Solution. Crystal Growth and Design, 2005, 5, 523-527.	3.0	133
13	Development of combined microstructure and structure characterization facility for <i>in situ</i> and <i>operando</i> studies at the Advanced Photon Source. Journal of Applied Crystallography, 2018, 51, 867-882.	4.5	129
14	Phase composition and its changes during annealing of plasma-sprayed YSZ. Surface and Coatings Technology, 2000, 127, 120-129.	4.8	126
15	Mitigation of PEM Fuel Cell Catalyst Degradation with Porous Carbon Supports. Journal of the Electrochemical Society, 2019, 166, F198-F207.	2.9	126
16	Microstructural characterization of yttria-stabilized zirconia plasma-sprayed deposits using multiple small-angle neutron scattering. Acta Materialia, 2001, 49, 1661-1675.	7.9	117
17	Monitoring simultaneously the growth of nanoparticles and aggregates byin situultra-small-angle x-ray scattering. Journal of Applied Physics, 2005, 97, 054309.	2.5	113
18	Three-Dimensional Coherent X-Ray Diffraction Imaging of a Ceramic Nanofoam: Determination of Structural Deformation Mechanisms. Physical Review Letters, 2008, 101, 055501.	7.8	106

#	Article	IF	CITATIONS
19	Influence of Spray Angle on the Pore and Crack Microstructure of Plasmaâ€Sprayed Deposits. Journal of the American Ceramic Society, 1997, 80, 733-742.	3.8	97
20	Investigation of the Interaction between Nafion Ionomer and Surface Functionalized Carbon Black Using Both Ultrasmall Angle X-ray Scattering and Cryo-TEM. ACS Applied Materials & Interfaces, 2017, 9, 6530-6538.	8.0	89
21	Evolution of the void structure in plasma-sprayed YSZ deposits during heating. Materials Science & Engineering A: Structural Materials: Properties, Microstructure and Processing, 1999, 272, 215-221.	5.6	88
22	Dehydration Effect on the Pore Size, Porosity, and Fractal Parameters of Shale Rocks: Ultrasmall-Angle X-ray Scattering Study. Energy & Fuels, 2014, 28, 6772-6779.	5.1	84
23	Effective pinhole-collimated ultrasmall-angle x-ray scattering instrument for measuring anisotropic microstructures. Review of Scientific Instruments, 2002, 73, 1660-1662.	1.3	81
24	Structure and dispersion of carbon nanotubes. Journal of Applied Crystallography, 2003, 36, 553-557.	4.5	80
25	Size-range analysis of diesel soot with ultra-small angle X-ray scattering. Combustion and Flame, 2004, 137, 63-72.	5.2	79
26	Small-angle X-ray and neutron scattering. Nature Reviews Methods Primers, 2021, 1, .	21.2	77
27	Effect of silica nanoparticles on morphology of segmented polyurethanes. Polymer, 2004, 45, 4285-4295.	3.8	75
28	X-ray scattering and spectroscopy studies on diesel soot from oxygenated fuel under various engine load conditions. Carbon, 2005, 43, 2588-2599.	10.3	71
29	Ultrahigh Molecular Weight Linear Block Copolymers: Rapid Access by Reversible-Deactivation Radical Polymerization and Self-Assembly into Large Domain Nanostructures. Macromolecules, 2016, 49, 3733-3738.	4.8	70
30	Changes in Pore Size Distribution upon Thermal Cycling of TATB-based Explosives Measured by Ultra-Small Angle X-Ray Scattering. Propellants, Explosives, Pyrotechnics, 2006, 31, 466-471.	1.6	69
31	Super-Stable, Highly Monodisperse Plasmonic Faradaurate-500 Nanocrystals with 500 Gold Atoms: Au _{â^1⁄4500} (SR) _{â^1⁄4120} . Journal of the American Chemical Society, 2014, 136, 7410-74	$1^{\frac{1}{7}3.7}_{.}$	67
32	Assessing the potential for CO2 adsorption in a subbituminous coal, Huntly Coalfield, New Zealand, using small angle scattering techniques. International Journal of Coal Geology, 2009, 77, 54-68.	5.0	63
33	Investigation of a Catalyst Ink Dispersion Using Both Ultra-Small-Angle X-ray Scattering and Cryogenic TEM. Langmuir, 2010, 26, 19199-19208.	3.5	62
34	In situ mechanical reinforcement of polymer hydrogels via metal-coordinated crosslink mineralization. Nature Communications, 2021, 12, 667.	12.8	60
35	<i>In situ</i> small-angle x-ray scattering study of nanostructure evolution during decomposition of arc evaporated TiAlN coatings. Applied Physics Letters, 2009, 94, .	3.3	59
36	Edible oil structures at low and intermediate concentrations. II. Ultra-small angle X-ray scattering of <i>in situ</i> tristearin solids in triolein. Journal of Applied Physics, 2013, 114, .	2.5	59

#	Article	IF	CITATIONS
37	NIST Standard Reference Material 3600: Absolute Intensity Calibration Standard for Small-Angle X-ray Scattering. Journal of Applied Crystallography, 2017, 50, 462-474.	4.5	57
38	Relationship between Self-Association of Glycine Molecules in Supersaturated Solutions and Solid State Outcome. Physical Review Letters, 2007, 99, 115702.	7.8	55
39	Measurement of carbon condensates using small-angle x-ray scattering during detonation of the high explosive hexanitrostilbene. Journal of Applied Physics, 2015, 117, .	2.5	55
40	Fast-responding bio-based shape memory thermoplastic polyurethanes. Polymer, 2017, 121, 26-37.	3.8	53
41	Measurements of droplet size in shear-driven atomization using ultra-small angle x-ray scattering. International Journal of Multiphase Flow, 2017, 92, 131-139.	3.4	53
42	Dedicated full-field X-ray imaging beamline at Advanced Photon Source. Nuclear Instruments and Methods in Physics Research, Section A: Accelerators, Spectrometers, Detectors and Associated Equipment, 2007, 582, 77-79.	1.6	52
43	Mesoscale evolution of voids and microstructural changes in HMX-based explosives during heating through the β-δ phase transition. Journal of Applied Physics, 2015, 118, .	2.5	52
44	Well-Ordered Polymer Melts with 5 nm Lamellar Domains from Blends of a Disordered Block Copolymer and a Selectively Associating Homopolymer of Low or High Molar Mass. Macromolecules, 2008, 41, 7978-7985.	4.8	51
45	Advanced Microstructural Characterization of Plasma-Sprayed Zirconia Coatings Over Extended Length Scales. Journal of Thermal Spray Technology, 2005, 14, 239-250.	3.1	50
46	Quantification of void networks of as-sprayed and annealed nanostructured yttria-stabilized zirconia (YSZ) deposits manufactured by suspension plasma spraying. Surface and Coatings Technology, 2010, 205, 683-689.	4.8	50
47	Porous Architecture of SPS Thick YSZ Coatings Structured at the Nanometer Scale (~50Ânm). Journal of Thermal Spray Technology, 2010, 19, 198-206.	3.1	49
48	In situ structural characterization of ageing kinetics in aluminum alloy 2024 across angstrom-to-micrometer length scales. Acta Materialia, 2016, 111, 385-398.	7.9	49
49	Thermal Spray Yttria-Stabilized Zirconia Phase Changes during Annealing. Journal of Thermal Spray Technology, 2001, 10, 497-501.	3.1	47
50	Phase structure in segmented polyurethanes having fatty acid-based soft segments. Polymer, 2013, 54, 372-380.	3.8	47
51	Challenges and opportunities in complex materials: silica-reinforced elastomers. Physica A: Statistical Mechanics and Its Applications, 2002, 314, 686-695.	2.6	46
52	Microstructural characterization studies to relate the properties of thermal-spray coatings to feedstock and spray conditions. Surface and Coatings Technology, 2001, 146-147, 544-552.	4.8	44
53	Alumina-base plasma-sprayed materials—Part II: Phase transformations in aluminas. Journal of Thermal Spray Technology, 1997, 6, 439-444.	3.1	42
54	Mechanisms for Lithium Nucleation and Dendrite Growth in Selected Carbon Allotropes. Chemistry of Materials, 2017, 29, 6205-6213.	6.7	42

#	Article	IF	CITATIONS
55	Advanced neutron and X-ray techniques for insights into the microstructure of EB-PVD thermal barrier coatings. Materials Science & Engineering A: Structural Materials: Properties, Microstructure and Processing, 2006, 426, 43-52.	5.6	41
56	Quantitative Measurement of Nanoparticle Halo Formation around Colloidal Microspheres in Binary Mixtures. Langmuir, 2008, 24, 6504-6508.	3.5	41
57	Microstructure-Property Correlations in Industrial Thermal Barrier Coatings. Journal of the American Ceramic Society, 2004, 87, 1294-1300.	3.8	40
58	High-energy ultra-small-angle X-ray scattering instrument at the Advanced Photon Source. Journal of Applied Crystallography, 2012, 45, 1318-1320.	4.5	39
59	Quantification of void network architectures of suspension plasma-sprayed (SPS) yttria-stabilized zirconia (YSZ) coatings using Ultra-small-angle X-ray scattering (USAXS). Materials Science & Engineering A: Structural Materials: Properties, Microstructure and Processing, 2010, 528, 91-102.	5.6	37
60	Ultra-Small-Angle X-ray Scattering of Polymers. Polymer Reviews, 2010, 50, 59-90.	10.9	37
61	Understanding Solvothermal Crystallization of Mesoporous Anatase Beads by In Situ Synchrotron PXRD and SAXS. Chemistry of Materials, 2014, 26, 4563-4571.	6.7	37
62	Nano-sized precipitate stability and its controlling factors in a NiAl-strengthened ferritic alloy. Scientific Reports, 2015, 5, 16081.	3.3	37
63	Impact of an Emergent Hierarchical Filler Network on Nanocomposite Dynamics. Macromolecules, 2018, 51, 7893-7904.	4.8	37
64	The Microstructure of TATBâ€Based Explosive Formulations During Temperature Cycling Using Ultraâ€6mallâ€Angle Xâ€Ray Scattering. Propellants, Explosives, Pyrotechnics, 2009, 34, 406-414.	1.6	36
65	Mercury intrusion porosimetry of plasma-sprayed ceramic. Journal of Materials Science, 1997, 32, 3925-3932.	3.7	35
66	The Absolute Calibration of a Small-Angle Scattering Instrument with a Laboratory X-ray Source. Journal of Physics: Conference Series, 2010, 247, 012005.	0.4	34
67	In-flight oxidation of high-alloy steels during plasma spraying. Materials Science & Engineering A: Structural Materials: Properties, Microstructure and Processing, 1999, 272, 199-206.	5.6	33
68	Polyphenols Weaken Pea Protein Gel by Formation of Large Aggregates with Diminished Noncovalent Interactions. Biomacromolecules, 2021, 22, 1001-1014.	5.4	33
69	Dispersing Grafted Nanoparticle Assemblies into Polymer Melts through Flow Fields. ACS Macro Letters, 2013, 2, 1051-1055.	4.8	32
70	Mesoscale Effects in Electrochemical Conversion: Coupling of Chemistry to Atomic- and Nanoscale Structure in Iron-Based Electrodes. Journal of the American Chemical Society, 2014, 136, 6211-6214.	13.7	32
71	Duplex Precipitates and Their Effects on the Room-temperature Fracture Behaviour of a NiAl-Strengthened Ferritic Alloy. Materials Research Letters, 2015, 3, 128-134.	8.7	31
72	Quantification of the coarsening kinetics of γ′ precipitates in Waspaloy microstructures with different prior homogenizing treatments. Acta Materialia, 2009, 57, 4658-4670.	7.9	30

#	Article	IF	CITATIONS
73	Location and distribution of inorganic material in a low ash yield, subbituminous coal. International Journal of Coal Geology, 2012, 94, 173-181.	5.0	30
74	Ordered array of <mml:math <br="" altimg="si18.gif" xmlns:mml="http://www.w3.org/1998/Math/MathML">overflow="scroll"><mml:mrow><mml:mi>Ï%</mml:mi></mml:mrow></mml:math> particles in <mml:math xmlns:mml="http://www.w3.org/1998/Math/MathML" altimg="si2.gif" overflow="scroll"><mml:mrow><mml:mi>β</mml:mi></mml:mrow>-Ti matrix studied by small-angle X-ray scattering. Acta Materialia, 2014, 81, 71-82.</mml:math 	7.9	30
75	Time–connectivity superposition and the gel/glass duality of weak colloidal gels. Proceedings of the National Academy of Sciences of the United States of America, 2021, 118, .	7.1	30
76	Low-temperature structural phase transition and incommensurate lattice modulation in the spin-gap compoundBaCuSi2O6. Physical Review B, 2006, 73, .	3.2	28
77	Selective imaging of nano-particle contrast agents by a single-shot x-ray diffraction technique. Optics Express, 2010, 18, 13271.	3.4	28
78	Effects of Ink Formulation on Construction of Catalyst Layers for High-Performance Polymer Electrolyte Membrane Fuel Cells. ACS Applied Materials & Interfaces, 2021, 13, 37004-37013.	8.0	28
79	Effect of chemical structure on the volume-phase transition in neutral and weakly charged poly(N-alkyl(meth)acrylamide) hydrogels studied by ultrasmall-angle x-ray scattering. Journal of Chemical Physics, 2006, 124, 234911.	3.0	27
80	Thermoplastic polyurethanes with controlled morphology based on methylenediphenyldiisocyanate/isosorbide/butanediol hard segments. Polymer International, 2015, 64, 1607-1616.	3.1	27
81	Experimental and Computational Investigation of Subcritical Near-Nozzle Spray Structure and Primary Atomization in the Engine Combustion Network Spray D. SAE International Journal of Fuels and Lubricants, 0, 11, 337-352.	0.2	27
82	Porous architecture and thermal properties of thermal barrier coatings deposited by suspension plasma spray. Surface and Coatings Technology, 2020, 386, 125462.	4.8	27
83	Mechanical reinforcement of polymer nanocomposites: theory and ultra-small angle X-ray scattering (USAXS) studies. Soft Matter, 2011, 7, 2725.	2.7	26
84	Hydration kinetics and morphology of cement pastes with pozzolanic volcanic ash studied via synchrotron-based techniques. Journal of Materials Science, 2018, 53, 1743-1757.	3.7	26
85	Structural Characterization of RDX-Based Explosive Nanocomposites. Propellants, Explosives, Pyrotechnics, 2013, 38, 386-393.	1.6	25
86	Effects of Ionic Strength, Salt, and pH on Aggregation of Boehmite Nanocrystals: Tumbler Small-Angle Neutron and X-ray Scattering and Imaging Analysis. Langmuir, 2018, 34, 15839-15853.	3.5	25
87	Polychromatic microdiffraction analysis of defect self-organization in shock deformed single crystals. International Journal of Plasticity, 2009, 25, 2081-2093.	8.8	24
88	Quantification of the physical structure of fats in 20 minutes: Implications for formulation. Lipid Technology, 2014, 26, 223-226.	0.3	24
89	Characterization of zein assemblies by ultra-small-angle X-ray scattering. Soft Matter, 2017, 13, 3053-3060.	2.7	24
90	<i>In situ</i> ultra-small-angle X-ray scattering study of the solution-mediated formation and growth of nanocrystalline ceria. Journal of Applied Crystallography, 2008, 41, 918-929.	4.5	23

#	Article	IF	CITATIONS
91	Atomic Structure of Au ₃₂₉ (SR) ₈₄ Faradaurate Plasmonic Nanomolecules. Journal of Physical Chemistry C, 2015, 119, 11260-11266.	3.1	23
92	Reference diffraction patterns, microstructure, and pore-size distribution for the copper (II) benzene-1,3,5-tricarboxylate metal organic framework (Cu-BTC) compounds. Powder Diffraction, 2015, 30, 2-13.	0.2	23
93	Supported Silver Nanoparticle and Near-Interface Solution Dynamics in a Deep Eutectic Solvent. Journal of Physical Chemistry C, 2016, 120, 1534-1545.	3.1	23
94	An <i>in situ</i> USAXS–SAXS–WAXS study of precipitate size distribution evolution in a model Ni-based alloy. Journal of Applied Crystallography, 2017, 50, 734-740.	4.5	23
95	Ultrasound-based formation of nano-Pickering emulsions investigated via in-situ SAXS. Journal of Colloid and Interface Science, 2019, 536, 281-290.	9.4	23
96	Lattice strain and damage evolution of 9–12%Cr ferritic/martensitic steel during in situ tensile test by X-ray diffraction and small angle scattering. Journal of Nuclear Materials, 2010, 407, 10-15.	2.7	22
97	Analysis of textural properties of CaO-based CO2 sorbents by ex situ USAXS. Chemical Engineering Journal, 2019, 355, 760-776.	12.7	22
98	Femtosecond quantification of void evolution during rapid material failure. Science Advances, 2020, 6, .	10.3	22
99	Development of ultra-small-angle X-ray scattering–X-ray photon correlation spectroscopy. Journal of Applied Crystallography, 2011, 44, 200-212.	4.5	21
100	Enhancement of scattering and reflectance properties of plasma-sprayed alumina coatings by controlling the porosity. Surface and Coatings Technology, 2013, 220, 80-84.	4.8	21
101	Structural and dynamical studies of acid-mediated conversion in amorphous-calcium-phosphate based dental composites. Dental Materials, 2014, 30, 1113-1125.	3.5	21
102	Programmable Anisotropy and Percolation in Supramolecular Patchy Particle Gels. ACS Nano, 2020, 14, 17018-17027.	14.6	21
103	Rapid structural and chemical characterization of ternary phase diagrams using synchrotron radiation. Journal of Materials Research, 2003, 18, 2522-2527.	2.6	20
104	Phase behavior of SEBS triblock copolymer gels. Journal of Polymer Science, Part B: Polymer Physics, 2011, 49, 1479-1491.	2.1	20
105	A thermal model to describe kinetic dispersion in rubber nanocomposites: The effect of mixing time on dispersion. Polymer, 2019, 175, 272-282.	3.8	19
106	Mechanisms of Ti <mml:math <br="" xmlns:mml="http://www.w3.org/1998/Math/MathML">altimg="si9.svg"><mml:msub><mml:mrow></mml:mrow><mml:mn>3</mml:mn></mml:msub></mml:math> Al precipitation in hcp <mml:math <br="" xmlns:mml="http://www.w3.org/1998/Math/MathML">altimg="si1.svg"><mml:mi>î±</mml:mi></mml:math> -Ti. Acta Materialia, 2021, 212, 116811.	7.9	19
107	Structure of Low-Density Nanoporous Dielectrics Revealed by Low-Vacuum Electron Microscopy and Small-Angle X-ray Scattering. Langmuir, 2007, 23, 353-356.	3.5	18
108	Nanocrystallization in spark plasma sintered Fe48Cr15Mo14Y2C15B6 bulk amorphous alloy. Journal of Applied Physics, 2013, 114, .	2.5	18

#	Article	IF	CITATIONS
109	Characterization of porosity in sulfide ore minerals: A USANS/SANS study. American Mineralogist, 2014, 99, 2398-2404.	1.9	18
110	Thermoplastic polyurethanes with isosorbide chain extender. Journal of Applied Polymer Science, 2015, 132, .	2.6	18
111	Use of small-angle X-ray scattering to resolve intracellular structure changes of <i>Escherichia coli</i> cells induced by antibiotic treatment. Journal of Applied Crystallography, 2016, 49, 2210-2216.	4.5	18
112	Resolving Detonation Nanodiamond Size Evolution and Morphology at Sub-Microsecond Timescales during High-Explosive Detonations. Journal of Physical Chemistry C, 2019, 123, 19153-19164.	3.1	18
113	Correlating inter-particle forces and particle shape to shear-induced aggregation/fragmentation and rheology for dilute anisotropic particle suspensions: A complementary study via capillary rheometry and in-situ small and ultra-small angle X-ray scattering. Journal of Colloid and Interface Science, 2020. 576. 47-58.	9.4	18
114	Fast nanoparticle rotational and translational diffusion in synovial fluid and hyaluronic acid solutions. Science Advances, 2021, 7, .	10.3	18
115	Heat accelerates degradation of β-lactoglobulin fibrils at neutral pH. Food Hydrocolloids, 2022, 124, 107291.	10.7	18
116	Water-Barrier Properties of Mixed Bis[trimethoxysilylpropyl]amine and Vinyltriacetoxysilane Films. Journal of Physical Chemistry B, 2007, 111, 7041-7051.	2.6	17
117	Application of USAXS analysis and non-interacting approximation to determine the influence of process parameters and ageing on the thermal conductivity of electron-beam physical vapor deposited thermal barrier coatings. Surface and Coatings Technology, 2007, 201, 4781-4788.	4.8	17
118	Microstructural evolution of 7wt.% Y2O3–ZrO2 thermal barrier coatings due to stress relaxation at elevated temperatures and the concomitant changes in thermal conductivity. Surface and Coatings Technology, 2010, 205, 57-65.	4.8	17
119	Wellbore Cement Porosity Evolution in Response to Mineral Alteration during CO2 Flooding. Environmental Science & Technology, 2017, 51, 692-698.	10.0	17
120	The effects of burial diagenesis on multiscale porosity in the St. Peter Sandstone: An imaging, small-angle, and ultra-small-angle neutron scattering analysis. Marine and Petroleum Geology, 2018, 92, 352-371.	3.3	17
121	Multiscale operando X-ray investigations provide insights into electro-chemo-mechanical behavior of lithium intercalation cathodes. Applied Energy, 2021, 299, 117315.	10.1	17
122	Depth-Resolved Porosity Investigation of EB-PVD Thermal Barrier Coatings Using High-Energy X-rays. Journal of the American Ceramic Society, 2004, 87, 268-274.	3.8	16
123	Self-assembly of carbon black into nanowires that form a conductive three dimensional micronetwork. Applied Physics Letters, 2007, 90, 014101.	3.3	16
124	High-temperature multifunctional magnetoactive nickel graphene polyimide nanocomposites. Polymer, 2013, 54, 2776-2784.	3.8	16
125	Quantification of Dispersion for Weakly and Strongly Correlated Nanofillers in Polymer Nanocomposites. Macromolecules, 2020, 53, 2235-2248.	4.8	16
126	Spatial heterogeneity analyses of pore structure and mineral composition of Barnett Shale using X-ray scattering techniques. Marine and Petroleum Geology, 2021, 134, 105354.	3.3	16

#	Article	IF	CITATIONS
127	Characterization of the closed porosity in plasma-sprayed alumina. Journal of Materials Science, 1997, 32, 3407-3410.	3.7	15
128	Extended hierarchical solvent perturbations from curved surfaces of mesoporous silica particles in a deep eutectic solvent. Journal of Colloid and Interface Science, 2018, 520, 81-90.	9.4	15
129	Extended range X-ray pair distribution functions. Nuclear Instruments and Methods in Physics Research, Section A: Accelerators, Spectrometers, Detectors and Associated Equipment, 2020, 955, 163318.	1.6	15
130	Influence of Silane Coupling Agents on Filler Network Structure and Stress-Induced Particle Rearrangement in Elastomer Nanocomposites. ACS Applied Materials & Interfaces, 2020, 12, 47891-47901.	8.0	15
131	Particle size analysis and characterization of nanodiamond dispersions in water and dimethylformamide by various scattering and diffraction methods. Journal of Nanoparticle Research, 2020, 22, 1.	1.9	15
132	Effect of Aging Treatment on the Microstructure and Resistivity of a Nickel-Base Superalloy. Metallurgical and Materials Transactions A: Physical Metallurgy and Materials Science, 2011, 42, 1362-1372.	2.2	14
133	Particle size distribution in ferrofluid macro-clusters. Journal of Magnetism and Magnetic Materials, 2013, 330, 31-36.	2.3	14
134	An Assessment of Milling Time on the Structure and Properties of a Nanostructured Ferritic Alloy (NFA). Metallurgical and Materials Transactions A: Physical Metallurgy and Materials Science, 2014, 45, 5409-5418.	2.2	14
135	A pseudo-thermodynamic description of dispersion for nanocomposites. Polymer, 2017, 129, 32-43.	3.8	14
136	In situ study of aggregate topology during growth of pyrolytic silica. Journal of Aerosol Science, 2018, 118, 34-44.	3.8	14
137	Phase Fraction and Evolution of Additively Manufactured (AM) 15-5 Stainless Steel and Inconel 625 AM-Bench Artifacts. Integrating Materials and Manufacturing Innovation, 2019, 8, 362-377.	2.6	14
138	Influence of microstructure on replacement and porosity generation during experimental dolomitization of limestones. Geochimica Et Cosmochimica Acta, 2021, 303, 137-158.	3.9	14
139	Versatile USAXS (Bonse-Hart) Facility for Advanced Materials Research. AIP Conference Proceedings, 2004, , .	0.4	13
140	Plasma spray coatings for producing next-generation supported membranes. Topics in Catalysis, 2005, 32, 241-249.	2.8	13
141	Nucleation of atomic-layer-deposited HfO2 films, and evolution of their microstructure, studied by grazing incidence small angle x-ray scattering using synchrotron radiation. Applied Physics Letters, 2006, 88, 032907.	3.3	13
142	Multiâ€scale Microstructure Characterization of Solid Oxide Fuel Cell Assemblies With Ultra Smallâ€Angle Xâ€Ray Scattering. Advanced Engineering Materials, 2009, 11, 495-501.	3.5	13
143	Characterization of Complex Thermal Barrier Deposits Pore Microstructures by a Combination of Imaging, Scattering, and Intrusion Techniques. Journal of Thermal Spray Technology, 2010, 19, 178-189.	3.1	13
144	Ultra-Small-Angle X-ray Scattering—X-ray Photon Correlation Spectroscopy: A New Measurement Technique for In-Situ Studies of Equilibrium and Nonequilibrium Dynamics. Metallurgical and Materials Transactions A: Physical Metallurgy and Materials Science, 2012, 43, 1445-1453.	2.2	13

#	Article	IF	CITATIONS
145	Structure and Dynamics Studies of Concentrated Micrometer-Sized Colloidal Suspensions. Langmuir, 2013, 29, 1379-1387.	3.5	13
146	A multi-length-scale USAXS/SAXS facility: 10–50 keV small-angle X-ray scattering instrument. Journal of Applied Crystallography, 2013, 46, 1508-1512.	4.5	13
147	BSMV as a Biotemplate for Palladium Nanomaterial Synthesis. Langmuir, 2017, 33, 1716-1724.	3.5	13
148	Effect of nanoparticles size and polyelectrolyte on nanoparticles aggregation in a cellulose fibrous matrix. Journal of Colloid and Interface Science, 2018, 510, 190-198.	9.4	13
149	Formation and Characterization of Zein-Based Oleogels. Journal of Agricultural and Food Chemistry, 2020, 68, 13276-13281.	5.2	13
150	Anisotropic Microstructure of Plasma-Sprayed Deposits. Journal of Thermal Spray Technology, 1999, 8, 414-420.	3.1	12
151	Morphology and water barrier properties of organosilane films: The effect of curing temperature. Journal of Colloid and Interface Science, 2006, 302, 287-293.	9.4	12
152	Quantitative characterization of the contrast mechanisms of ultra-small-angle X-ray scattering imaging. Journal of Applied Crystallography, 2008, 41, 416-427.	4.5	12
153	Kinetic transition in the growth of Al nanocrystals in Al-Sm alloys. Journal of Applied Physics, 2012, 111, 063525.	2.5	12
154	Topological investigation of electronic silicon nanoparticulate aggregates using ultra-small-angle X-ray scattering. Journal of Nanoparticle Research, 2012, 14, 1.	1.9	12
155	Nanoparticle scaffolds for syngas-fed solid oxide fuel cells. Journal of Materials Chemistry A, 2015, 3, 3011-3018.	10.3	12
156	Plasma-sprayed aluminium coating. Journal of Materials Science Letters, 1992, 11, 573-574.	0.5	11
157	Investigation of Solvent Effects on the Dispersion of Carbon Agglomerates and Nafion Ionomer Particles in Catalyst Inks Using Ultra Small Angle X-Ray Scattering Method. ECS Transactions, 2016, 75, 361-371.	0.5	11
158	A SAXS-WAXS study of the endothermic transitions in amorphous or supercooled liquid itraconazole. Thermochimica Acta, 2016, 644, 1-5.	2.7	11
159	Surface Pb Nanoparticle Aggregation, Coalescence and Differential Capacitance in a Deep Eutectic Solvent Using a Simultaneous Sample-Rotated Small Angle X-ray Scattering and Electrochemical Methods Approach. Electrochimica Acta, 2017, 228, 462-473.	5.2	11
160	Nanostructured Thermoset/Thermoset Blends Compatibilized with an Amphiphilic Block Copolymer. Macromolecules, 2019, 52, 3104-3114.	4.8	11
161	Crystallization Mechanism in Spark Plasma Sintered Bulk Metallic Glass Analyzed using Small Angle Neutron Scattering. Scientific Reports, 2020, 10, 2033.	3.3	11
162	Microstructure-Wear and -Corrosion Relationships for Thermally Sprayed Metallic Deposits. , 2000, , .		11

#	Article	IF	CITATIONS
163	Small-angle neutron scattering study of the role of feedstock particle size on the microstructural behavior of plasma-sprayed yttria-stabilized zirconia deposits. Journal of Materials Research, 2003, 18, 624-634.	2.6	10
164	Ostwald ripening of cobalt precipitates in silica aerogels? An ultra-small-angle X-ray scattering study. Journal of Applied Crystallography, 2005, 38, 132-138.	4.5	10
165	Complex pore spaces create record-breaking methane storage system for natural-gas vehicles. Chaos, 2007, 17, 041108.	2.5	10
166	Processâ€Controlled Plasmaâ€6prayed Yttriaâ€6tabilized Zirconia Coatings: New Insights from Ultrasmallâ€Angle Xâ€ray Scattering. Journal of the American Ceramic Society, 2009, 92, 491-500.	3.8	10
167	Effect of Al on the NiAl-Type B2 Precipitates in Ferritic Superalloys. Metallurgical and Materials Transactions A: Physical Metallurgy and Materials Science, 2012, 43, 3423-3427.	2.2	10
168	Evolution of electrochemical interfaces in solid oxide fuel cells (SOFC): a Ni and Zr resonant anomalous ultra-small-angle X-ray scattering study with elemental and spatial resolution across the cell assembly. RSC Advances, 2014, 4, 4676-4690.	3.6	10
169	Structural characterization of solid lipoproteic colloid gels by ultra-small-angle X-ray scattering and the relation with sodium release. Food Hydrocolloids, 2016, 56, 325-333.	10.7	10
170	Inverse transformation: unleashing spatially heterogeneous dynamics with an alternative approach to XPCS data analysis. Journal of Applied Crystallography, 2018, 51, 35-46.	4.5	10
171	Controls of Microstructure and Chemical Reactivity on the Replacement of Limestone by Fluorite Studied Using Spatially Resolved Small Angle X-ray and Neutron Scattering. ACS Earth and Space Chemistry, 2019, 3, 1998-2016.	2.7	10
172	Recent Developments in the Characterization of Anisotropic Void Populations in Thermal Barrier Coatings Using Ultra-Small Angle X-Ray Scattering. , 0, , 517-524.		10
173	Structural evolution during gelation of pea and whey proteins envisaged by time-resolved ultra-small-angle x-ray scattering (USAXS). Food Hydrocolloids, 2022, 126, 107449.	10.7	10
174	Relation of the fractal structure of organic pigments to their performance. Journal of Applied Physics, 2002, 91, 6120-6124.	2.5	9
175	In-Flight Alloying of Nanocrystalline Yttria-Stabilized Zirconia Using Suspension Spray to Produce Ultra-Low Thermal Conductivity Thermal Barriers. International Journal of Applied Ceramic Technology, 2011, 8, 1382-1392.	2.1	9
176	Ultraâ€smallâ€angle Xâ€fay scattering–Xâ€fay photon correlation spectroscopy studies of incipient structural changes in amorphous calcium phosphateâ€based dental composites. Journal of Biomedical Materials Research - Part A, 2012, 100A, 1293-1306.	4.0	9
177	Synchrotron X-ray studies of model SOFC cathodes, part I: Thin film cathodes. Solid State Ionics, 2017, 311, 118-126.	2.7	9
178	Diversifying Composition Leads to Hierarchical Composites with Design Flexibility and Structural Fidelity. ACS Nano, 2021, 15, 14095-14104.	14.6	9
179	Ultrasmall-angle X-ray scattering (USAXS) studies of morphological trends in high energy milled NaAlH4 powders. Journal of Alloys and Compounds, 2007, 446-447, 248-254.	5.5	8
180	Small angle X-ray scattering analysis of the effect of cold compaction of Al/MoO ₃ thermite composites. Physical Chemistry Chemical Physics, 2008, 10, 193-199.	2.8	8

#	Article	IF	CITATIONS
181	<i>CONTIN XPCS</i> : software for inverse transform analysis of X-ray photon correlation spectroscopy dynamics. Journal of Applied Crystallography, 2018, 51, 205-209.	4.5	8
182	X-RAY MEASUREMENTS OF FUEL SPRAY SPECIFIC SURFACE AREA AND SAUTER MEAN DIAMETER FOR CAVITATING AND NON-CAVITATING DIESEL SPRAYS. Atomization and Sprays, 2019, 29, 199-216.	0.8	8
183	Parametric Analysis and Modeling for the Porosity Prediction in Suspension Plasma-Sprayed Coatings. Journal of Thermal Spray Technology, 2020, 29, 51-59.	3.1	8
184	Chemical inhomogeneity of silicates treated by plasma spraying. Journal of Analytical Atomic Spectrometry, 1999, 14, 471-473.	3.0	7
185	Deformation of diesel soot aggregates as a function of pellet pressure: A study with ultra-small-angle x-ray scattering. Journal of Applied Physics, 2005, 98, 073513.	2.5	7
186	Structure and Dynamics of Bimodal Colloidal Dispersions in a Low-Molecular-Weight Polymer Solution. Langmuir, 2017, 33, 2817-2828.	3.5	7
187	Noninvasive detection of nanoparticle clustering by water proton NMR. Translational Materials Research, 2017, 4, 025002.	1.2	7
188	Designing CO ₂ -Responsive Multifunctional Nanoscale Fluids with Tunable Hydrogel Behavior for Subsurface Energy Recovery. Energy & Fuels, 2019, 33, 5988-5995.	5.1	7
189	The effects of staged mixing on the dispersion of reinforcing fillers in elastomer compounds. Polymer, 2019, 181, 121765.	3.8	7
190	Synthesis and characterization of polylactideâ€PAMAM "Janusâ€ŧype―linearâ€dendritic hybrids. Journal of Polymer Science Part A, 2019, 57, 1448-1459.	2.3	7
191	Evaluation of nano/submicro pores in suspension plasma sprayed YSZ coatings. Surface and Coatings Technology, 2019, 378, 125001.	4.8	7
192	Pressure-Thresholded Response in Cylindrically Shocked Cyclotrimethylene Trinitramine (RDX). Journal of Physical Chemistry A, 2020, 124, 3301-3313.	2.5	7
193	Manipulating meso-scale solvent structure from Pd nanoparticle deposits in deep eutectic solvents. Journal of Chemical Physics, 2021, 155, 074505.	3.0	7
194	The ultra-small-angle X-ray scattering instrument on UNICAT at the APS. AIP Conference Proceedings, 2000, , .	0.4	6
195	Characterisation of thermally sprayed metallic NiCrAlY deposits by multiple small-angle scattering. Applied Physics A: Materials Science and Processing, 2002, 74, s975-s977.	2.3	6
196	Applications of Laminar Weak-Link Mechanisms for Ultraprecision Synchrotron Radiation Instruments. AIP Conference Proceedings, 2007, , .	0.4	6
197	Highly porous activated glassy carbon film sandwich structure for electrochemical energy storage in ultracapacitor applications: Study of the porous film structure and gradient. Journal of Materials Research, 2010, 25, 1532-1540.	2.6	6
198	Investigation of condensed supercritical ethylene jets using Small Angle X-ray Scattering (SAXS) technique. Nuclear Instruments and Methods in Physics Research, Section A: Accelerators, Spectrometers, Detectors and Associated Equipment, 2011, 649, 219-221.	1.6	6

#	Article	IF	CITATIONS
199	Manufacturing and characterization of Ni-free N-containing ODS austenitic alloy. Journal of Nuclear Materials, 2018, 501, 72-81.	2.7	6
200	Extending synchrotron SAXS instrument ranges through addition of a portable, inexpensive USAXS module with vertical rotation axes. Journal of Synchrotron Radiation, 2021, 28, 824-833.	2.4	6
201	X-Ray Characterization of Real Fuel Sprays for Gasoline Direct Injection. Journal of Energy Resources Technology, Transactions of the ASME, 2022, 144, .	2.3	6
202	Solid-State Transformation of an Additive Manufactured Inconel 625 Alloy at 700 °C. Applied Sciences (Switzerland), 2021, 11, 8643.	2.5	6
203	Application of Ce for scavenging Cu impurities in A356 Al alloys. European Journal of Materials, 2021, 1, 3-18.	2.6	6
204	Development of Nanocrystalline Graphite from Lignin Sources. ACS Sustainable Chemistry and Engineering, 2022, 10, 1786-1794.	6.7	6
205	Robust nanoporous alumina monoliths by atomic layer deposition on low-density carbon-nanotube scaffolds. Carbon, 2014, 73, 443-447.	10.3	5
206	Magnetic-field-dependent assembly of silica-coated magnetite nanoclusters probed by Ultra-Small-Angle X-ray Scattering (USAXS). Journal of Magnetism and Magnetic Materials, 2014, 354, 70-75.	2.3	5
207	Comparative structural investigations of nuclear waste glass alteration layers and sol-gel synthesized aerogels. Npj Materials Degradation, 2020, 4, .	5.8	5
208	Engineering Calcium-Bearing Mineral/Hydrogel Composites for Effective Phosphate Recovery. ACS ES&T Engineering, 2021, 1, 1553-1564.	7.6	5
209	Ultra-high gamma irradiation of calcium silicate hydrates: Impact on mechanical properties, nanostructure, and atomic environments. Cement and Concrete Research, 2022, 158, 106855.	11.0	5
210	Multiple small-angle neutron scattering studies of anisotropic materials. Applied Physics A: Materials Science and Processing, 2002, 74, s937-s939.	2.3	4
211	Versatile Collimating Crystal Stage for a Bonse-Hart USAXS Instrument. AIP Conference Proceedings, 2007, , .	0.4	4
212	Annealing behavior of atomic layer deposited HfO2 films studied by synchrotron x-ray reflectivity and grazing incidence small angle scattering. Journal of Applied Physics, 2009, 105, 103522.	2.5	4
213	Simultaneous multiplexed materials characterization using a high-precision hard X-ray micro-slit array. Journal of Synchrotron Radiation, 2015, 22, 653-660.	2.4	4
214	Probing He bubbles in naturally aged and annealed δ-Pu alloys using ultra-small-angle x-ray scattering. Journal of Nuclear Materials, 2018, 498, 505-510.	2.7	4
215	High-Resolution Comonomer Sequencing of Blocky Brominated Syndiotactic Polystyrene Copolymers Using ¹³ C NMR Spectroscopy and Computer Simulations. Macromolecules, 2020, 53, 9539-9552.	4.8	4
216	Characterization of ferrogels prepared using $\hat{1}^3$ -Fe 2 O 3 and Fe 3 O 4 nanoparticles. , 2009, , .		3

#	Article	IF	CITATIONS
217	Investigation of Droplet Nucleation Inside Supercritical Ethylene Jets Using Small Angle X-Ray Scattering (SAXS) Technique. , 2010, , .		3
218	Reference diffraction patterns, microstructure, and pore-size distribution for the copper (II) benzene-1,3,5-tricarboxylate metal organic framework (Cu-BTC) compounds – CORRIGENDUM. Powder Diffraction, 2015, 30, 323-323.	0.2	3
219	Dispersed SiC nanoparticles in Ni observed by ultra-small-angle X-ray scattering. Journal of Applied Crystallography, 2016, 49, 2155-2160.	4.5	3
220	Synthesis and synchrotron characterisation of novel dual-template of hydroxyapatite scaffolds with controlled size porous distribution. Materials Letters, 2017, 190, 107-110.	2.6	3
221	Synchrotron X-ray studies of model SOFC cathodes, part II: Porous powder cathodes. Solid State Ionics, 2017, 311, 127-131.	2.7	3
222	3D Volumetric Structural Hierarchy Induced by Colloidal Polymerization of a Quantum-Dot Ionic Liquid Monomer Conjugate. Macromolecules, 2020, 53, 2822-2833.	4.8	3
223	Characterization of Solid Oxide Fuel Cell Layers by Computed X-Ray Microtomography and Small-Angle Scattering. Ceramic Engineering and Science Proceedings, 0, , 275-280.	0.1	3
224	Changes in the Microstructure of Plasma-Sprayed Yttria-Stabilized Zirconia Deposits during Simulated Operating Conditions. , 1997, , .		3
225	Residual Stress Evolution during Decomposition of Ti _(1-x) Al _(x) N Coatings Using High-Energy X-Rays. Materials Science Forum, 2006, 524-525, 619-624.	0.3	2
226	Ultra Small Angle X-ray Scattering Studies of Solid Oxide Fuel Cell Cathode Powders. ECS Transactions, 2013, 50, 111-115.	0.5	2
227	Explorations and 3D models of Atmospheric and Suspension Plasma Spraying coating microstructure. Surface and Coatings Technology, 2015, 268, 266-271.	4.8	2
228	High-efficiency coherence-preserving harmonic rejection with crystal optics. Journal of Synchrotron Radiation, 2018, 25, 1354-1361.	2.4	2
229	Effect of post annealing on microstructure and mechanical properties in Ni-free N-containing ODS steel. Materials Characterization, 2019, 153, 339-347.	4.4	2
230	Elastic Modulus Measurements in Plasma Sprayed Deposits. , 1997, , .		2
231	Water-Stabilized Plasma Spray Technology Offers Higher Production Rates at Lower Cost. Materials Technology, 1998, 13, 56-58.	3.0	1
232	Correlating Small Angle Scattering Spectra to Electrical Resistivity Changes in a Nickel-base Superalloy. Materials Research Society Symposia Proceedings, 2010, 1262, 1.	0.1	1
233	Effects of Back Pressure on Condensed-Phase Properties Within Supercritical Ethylene Jets. , 2011, , .		1

#	Article	IF	CITATIONS
235	Ultra-small-angle X-ray scattering study of second-phase particles in heat-treated Zircaloy-4. Journal of Applied Crystallography, 2015, 48, 52-60.	4.5	1
236	Quantification of Thermal Oxidation in Metallic Glass Powder using Ultra-small Angle X-ray Scattering. Scientific Reports, 2019, 9, 6836.	3.3	1
237	How Do Orientation Fluctuations Evolve to Crystals?. , 2007, , 117-132.		1
238	Evolution of the Microstructure of Plasma-Sprayed Deposits During Heating. , 1998, , .		1
239	Aerosol-Assisted Deposition for TiO2 Immobilization on Photocatalytic Fibrous Filters for VOC Degradation. Frontiers in Chemistry, 2022, 10, .	3.6	1
240	A novel SAXS model for multi-texture systems: application to CaCO3 calcination using in-situ USAXS-SAXS-WAXS. Applied Materials Today, 2022, 29, 101568.	4.3	1
241	Evaluation of High-Resolution SANS Measurements in Multiple Scattering Regime. Materials Science Forum, 2000, 321-324, 270-275.	0.3	Ο
242	A Comparative Study of Characteristics of Ferrogels Prepared using Coated and Uncoated Fe3O4 Nanoparticles. Materials Research Society Symposia Proceedings, 2009, 1234, 1.	0.1	0
243	Characterization of Fe3O4 and Fe2O3 ferrogels prepared under uniform magnetic field. Materials Research Society Symposia Proceedings, 2012, 1403, 214.	0.1	0
244	Ultra Small Angle X-Ray Scattering Characterization of Temperature-Sensitive Ferrogels Prepared Using Magnetic Nanoparticles. Materials Research Society Symposia Proceedings, 2013, 1453, 40.	0.1	0
245	High-Performance Pt Catalysts Supported on High-Surface-Area Graphene Composites for PEFCs. ECS Transactions, 2013, 50, 1453-1459.	0.5	Ο
246	Mapping of Microbial Habitats in Organic-Rich Shale. , 2015, , .		0
247	Anomalous Anisotropic Nanoparticle Aggregation in Cu ₂ (OH) ₃ Br Gels. Langmuir, 2020, 36, 8311-8321.	3.5	0
248	Phase Composition of Plasma-Sprayed Yttria Stabilized Zirconia. , 1997, , .		0
249	Evolution of α phase in metastable β titanium alloys studied by small-angle X-ray scattering. MATEC Web of Conferences, 2020, 321, 12039.	0.2	0
250	Relation of Thermal Conductivity with Process Induced Anisotropic Void Systems in EB-PVD PYSZ Thermal Barrier Coatings. Ceramic Engineering and Science Proceedings, 0, , 2-15.	0.1	0